Proposal for low-power atom trapping on a GaN-on-sapphire chip

Aiping Liu,[1,4] Lei Xu,[2,5] Xin-Biao Xu,[2,5] Guang-Jie Chen,[2,5] Pengfei Zhang,[3] Guo-Yong Xiang,[2,5] Guang-Can Guo,[2,5] Qin Wang,[1,4,*] and Chang-Ling Zou[2,3,5,†]

[1]*Institute of Quantum Information and Technology, Nanjing University of Posts and Telecommunications, Nanjing 210003, China*
[2]*CAS Key Laboratory of Quantum Information, University of Science and Technology of China, Hefei 230026, China*
[3]*State Key Laboratory of Quantum Optics and Quantum Optics Devices and Institute of Opto-Electronics, Shanxi University, Taiyuan 030006, China*
[4]*Broadband Wireless Communication and Sensor Network Technology, Key Laboratory of Ministry of Education, Nanjing University of Posts and Telecommunications, Nanjing 210003, China*
[5]*CAS Center for Excellence in Quantum Information and Quantum Physics, University of Science and Technology of China, Hefei 230026, China*

(Received 24 May 2022; revised 4 August 2022; accepted 29 August 2022; published 7 September 2022)

Hybrid photon-atom integrated circuits, which include photonic microcavities and trapped single neutral atoms in their evanescent field, have great potential for quantum information processing. In this platform, the atoms provide single-photon nonlinearity and long-lived memory, which are complementary to the excellent passive photonic devices in conventional quantum photonic circuits. In this work, we propose a stable platform for realizing hybrid photon-atom circuits based on an unsuspended photonic chip. By introducing high-order modes in the microring, a feasible evanescent-field trap potential well ∼0.26 mK could be obtained by only 10-mW-level power in the cavity, compared with the 100-mW-level power required in the scheme based on fundamental modes. Based on our scheme, stable single-atom trapping with relatively low laser power is feasible for future studies on high-fidelity quantum gates, single-photon sources, and many-body quantum physics based on a controllable atom array in a microcavity.

DOI: 10.1103/PhysRevA.106.033104

I. INTRODUCTION

With high scalability and enhanced light-matter interactions, the integrated quantum photonic chip has become a promising technology for the study of quantum optics and quantum information processing [1–3]. In recent decades, great progress has been achieved in photonic integrated circuits (PICs), with most attention being paid to excellent photonic material platforms [4–7]. Various quantum photonic devices with passive components and probabilistic state generation are demonstrated, with single emitters strongly desired for single-photon-level optical nonlinearity, which is an essential resource for quantum light sources and deterministic quantum operations [8]. Neutral atoms with long-lived energy levels provide a potential solution for the essential single-level nonlinearity to the PIC, which could also provide long-coherence time memory for storing quantum information. In addition, quantum computing and quantum sensing based on atoms can also be performed with the help of nanophotonic devices [9,10].

Since there is a promising prospect for the photon-atom interaction on a PIC, considerable efforts have recently been devoted to combining nanophotonic devices and neutral atoms to realize efficient quantum devices. Although much exciting progress has been achieved with the probabilistic strong coupling between optical microcavities [11–13], it is important to realize stable quantum photonic devices to trap atoms in nanophotonic devices. Various approaches have been developed to use near-field optical dipole traps to confine atoms at the surface of waveguide structures, including nanofibers [14–16], optical waveguides [17–20], photonic crystal nanocavities [21–23], and microsphere resonators [24]. However, these structures are suspended in a vacuum, so they are potentially sensitive to vibrations and vulnerable to thermal instability. Alternatively, atom trapping by unsuspended waveguide and microring structures has been proposed [25–27] and demonstrated [28–30]. These studies on trapping atoms promote the realization of a stable and scalable hybrid PIC on a substrate for future applications.

In this work, a stable platform for realizing a hybrid photon-atom circuit based on a suspension-free gallium nitride (GaN) chip is proposed. The sapphire substrate is transparent to visible lasers, thus allowing efficient optical access for laser cooling and an optical conveyor belt of cold atoms. To trap atoms, high-order guided modes in the microring waveguide are used to obtain a stable atom trapping near the surface of the microring. The required power to trap light using hybrid mode trapping is reduced compared to that of fundamental mode trapping. The manipulation of the atom states with the waveguide mode is analyzed numerically, which indicates a strong interaction between the trapped atom and the confined optical photons through the evanescent field

*qinw@njupt.edu.cn
†clzou321@ustc.edu.cn

 ©2022 American Physical Society

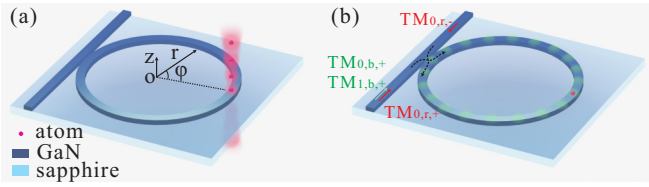

FIG. 1. Illustration of the microring platform for photon-atom interaction. (a) The microring platform with the atoms loaded on the surface of the microring by the free-space laser beam. (b) The microring platform with the atoms trapped on the surface of the microring by the optical evanescent fields formed by the guiding modes.

of the waveguide mode. Such a GaN-on-sapphire platform is feasible for hybrid photon-atom circuits and is promising for various quantum photonic devices.

II. THE PLATFORM FOR THE HYBRID PHOTON-ATOM CIRCUIT

The proposed experimental platform for hybrid photon-atom circuits is illustrated in Fig. 1. The platform is made of GaN microrings and waveguides on a sapphire substrate, which is transparent to visible light. Such a platform has been extensively studied in the past few decades, showing its excellent optical properties at visible wavelengths [31–35] and its potential in photonic integrated circuits [36,37]. Distinct from the conventional platforms for photon-atom interaction on a silicon substrate, all the photonic microstructures in our system are fabricated on the substrate, without any suspended structure or any fabrication procession of the substrate. The hybrid photon-atom circuits are prepared in three steps.

(i) Place the GaN-on-sapphire chip in vacuum. Since all the materials are transparent to visible light, the conventional magneto-optical trap can be implemented by transmitting laser beams through the chip. A cloud of cold atoms can be prepared by Doppler cooling, with the atomic cloud being only a few millimeters away from the top surface of the microring device.

(ii) Guide the cold atoms to the chip. By sending a pair of counterpropagating focused Gaussian beams of red-detuned laser vertically through the transparent substrate, with the waist of the laser beams being close to the microring on the chip, the cold atoms can be trapped and transported to the top surface of the microring by the optical conveyor belt [38,39]. As illustrated in Fig. 1(a), by tuning the phase of upward and downward dipole laser beams, atoms can be guided and transported to the chip.

(iii) When the cold atoms are guided to a certain distance from the top surface of the microring, turn on the blue- and red-detuned lasers in the photonic integrated circuits, thus creating the two-color optical dipole trap [27,40–42] via the evanescent fields of the microring resonator. Then, the single atoms can be confined to the microring resonator, as shown in Fig. 1(b), and coupled to the signal photons near the transition frequency of the atoms.

Following this procedure, our platform offers a basic cavity-QED system for realizing atom-photon quantum gates, atom-mediated photon-photon entanglement, and quantum storage. It is also worth noting that the materials of this platform hold several advantages. First, the unsuspended photonic circuit platform is very stable and is robust to external mechanical perturbations and thermal instability. In particular, to provide a deep trap for atoms using the evanescent field, a strong laser intensity in the microring should be excited, which will result in serious heating [43,44]. Second, since GaN and sapphire are wide-band-gap (0.78–4.77 eV) materials transparent to ultrabroadband wavelengths (260–1590 nm) [45,46], the scheme is valid for most atoms working with visible and near-visible lasers. Third, for atomic transitions at visible wavelengths, the refractive indices of GaN and the substrate are approximately $n_1 = 2.2$ and $n_2 = 1.7$, respectively. The large refractive index contrast indicates strong optical confinement in the GaN microphotonic structures [47]. Last, GaN is not only promising for nonlinear photonics with large intrinsic nonlinearities and a large band gap but also quite resilient to high temperature and optical power. Therefore, the GaN microring can sustain a relatively high intracavity optical power for the efficient manipulation of the neutral atoms.

As all the essential components and techniques of the hybrid photon-atom circuit are feasible for experiments, we focus on the design of the photonic structure for reasonable dipole traps and for strong photon-atom interactions. Therefore, in the following, we will investigate the performance of the dipole trap in detail and the potential photon-atom coupling strength.

III. THE SIMULATION OF THE TRAP POTENTIAL WELL

In this work, we consider rubidium atoms with a D_2 transition wavelength of ^{87}Rb atoms $\lambda_0 = 780$ nm. The optical properties of the GaN microring are determined by the geometry, which can be described by the major radius R, width w, and height h of the cross section of the microring, as shown in the top part of Fig. 2(a), where $R = 10\,\mu$m, $w = 600$ nm, and $h = 280$ nm. Two lasers, with wavelengths $\lambda_b = 760$ nm and $\lambda_r = 852$ nm, serve as the blue- and red-detuned dipole trap light [27,40–42]. When the two lasers are loaded into the microring, the excited microring modes can enhance the electric field and their evanescent parts in vacuum to offer the trap potential. The evanescent field decays exponentially away from the surface of the microring, so it provides a repulsive force and an attractive force on the considered ^{87}Rb atom through the blue- and red-detuned light modes, respectively. In addition, the attractive van der Waals force increases rapidly when the atom is close to the surface of the microring; thus, the atoms will stick to the surface [48]. Benefiting from the resonance enhancement of the microring, a strong evanescent field can be obtained with a relatively weak laser input to compensate for the van der Waals force. In the following studies, a trap potential composed of the optical dipole potential and the van der Waals potential is considered. By appropriately manipulating the incident light, a stable potential well for trapping ^{87}Rb atoms can be formed with a trap center about 100 nm away from the microring waveguide surface.

There are different waveguide modes in the microring waveguide, as illustrated in the inset in Fig. 2(a): the electric-field distributions of the fundamental modes TM_0 and TE_0, as well as the high-order modes TM_1 and TE_1 [49], for

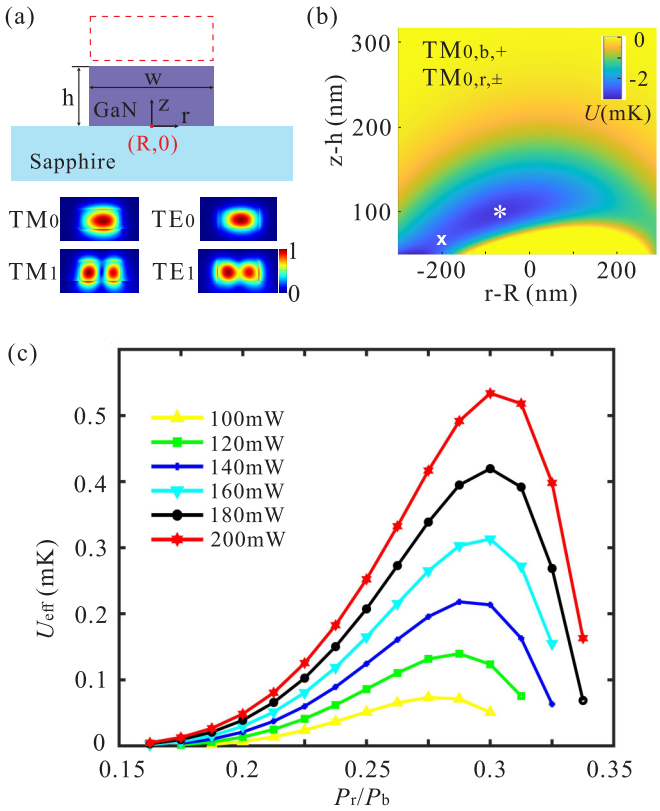

FIG. 2. The optical trap formed with the fundamental waveguide mode of the microring. (a) The cross section of the microring (top) and the optical-field distributions of the propagating modes in the microring (bottom). (b) The optical potential distribution formed by the fundamental modes in the r-z plane above the microring surface. (c) The optical traps vary with P_r/P_b for different P_b.

incident light wavelength λ_b. In the cylindrical coordinate system shown in Fig. 1(a), the TM (TE) mode of the microring waveguide is defined with its magnetic (electric) field parallel to r. The optical-field distribution on the microring waveguide is simulated by the finite-element method. Compared with TE modes, TM modes have a stronger evanescent field on the top surface of the waveguide, so only TM modes are considered in the following. Because of the material and geometry dispersion, the orbit angular momenta of the blue- and red-detuned circulating modes are different, and the standing-wave potential wells of the two lasers could not be matched in the microring. Therefore, only one trap laser, i.e., the red-detuned TM_0 mode, is bidirectionally excited with the same laser power to form a standing wave, as shown in Fig. 1(b). The details of calculating the atom trap potential are given in Appendix A.

Shown in Fig. 2(b) is the simulated trap potential formed on top of the microring in the simplest case in which the fundamental mode TM_0 is excited for blue- and red-detuned lasers, which are denoted by $TM_{0,b,+}$ and $TM_{0,r,\pm}$, with the indices + and − being the excitation directions of the waveguide modes. The optical trap in Fig. 2(b) is on the antinode cross section of the standing wave formed by the bidirectional circulating $TM_{0,r}$ modes corresponding to the dashed rectangle in Fig. 2(a). Similar to the pioneering studies in Ref. [27], the trap potential well is a narrow crescent because of the asymmetric field distributions of the microring modes on the microring cross section. An effective trap potential of 0.261 mK (the potential difference between the trap center and the saddle point) is obtained on the designed platform with $P_b = 150$ mW and $P_r = 43.3$ mW, which are the unidirectional laser powers for TM_{0b} and TM_{0r}, respectively. The center $T(r - R = -73\,\text{nm}, z - h = 100\,\text{nm})$ of the trap potential well is marked by the white asterisk, and the saddle point $A(r - R = -203\,\text{nm}, z - h = 68\,\text{nm})$ is marked by the white cross. It is worth noting that the potential is evaluated for a given intracavity power, which should be much higher than the input power in the waveguide due to the resonant enhancement by the microring cavity modes. For example, with a practical intrinsic quality factor of $Q \approx 2 \times 10^6$ for a critically coupled microring cavity [35,47], the required input laser power to the microring could be only approximately 0.2 mW.

The dependence of the optical trap depth U_{eff} on the power of the circulating laser power inside the microring is shown in Fig. 2(c). The curves illustrate the optical trap depth U_{eff} varying with the power ratio of red- and blue-detuned TM_0 modes P_r/P_b, and the different curves correspond to the power of the blue-detuned TM_0 mode as 100, 120, 140, 160, 180, and 200 mW. From Fig. 2(c), the optical trap depth not only increases with P_b but is also related to P_r/P_b. With a constant P_b, the optical trap depth U_{eff} increases at first and then decreases when P_r/P_b increases. Since the optimal optical trap is formed by the repulsive force due to the blue-detuned evanescent field and the attraction force due to the red-detuned evanescent field, as well as the van der Waals force, there is an optimal P_r/P_b to form the maximum optical trap depth when the balance between these forces is achieved. Because the van der Waals force is almost fixed for an optimal trap location approximately 100 nm above the surface, more red-tuned laser power is required to achieve balance when the blue-detuned laser power P_b increases, and the optimal P_r/P_b increases with P_b, as shown in Fig. 2(c). In fact, the optical trap cannot be formed when P_r/P_b is too small or too large, especially with low mode power. In addition to high enough intracavity powers, an appropriate P_r/P_b is also required to form a large effective optical trap depth U_{eff}.

From the trap potential distribution in Fig. 2(b), the effective trap depth is limited by the relatively low trap depth at the saddle point. To further reduce the required laser power, we should improve the trap depth at the saddle point and obtain a more regular optical trap potential well. Therefore, a set of hybrid modes composed of the blue-detuned TM_0 mode, red-detuned TM_0 mode, and blue-detuned TM_1 mode is used to form the optical trap potential well [50]. Figure 3(a) shows the optical trap potential well formed with these hybrid modes on the antinode cross section of the blue-detuned standing wave corresponding to the dashed rectangle in Fig. 2(a). The saddle point of the optical trap well has a much higher potential barrier because the optical field of the assisted TM_1 mode makes up the weak field on the two sides of the TM_0 mode, as shown in Fig. 2(a). The optical trap depth, with the trap center $T(r - R = 6\,\text{nm}, z - h = 100\,\text{nm})$ marked by the black asterisk and the saddle point $A(r - R = -216\,\text{nm}, z - h = 111\,\text{nm})$ marked by the black cross, is approximately 0.256 mK, with $P_b = 15.0$ mW, $P_r =$

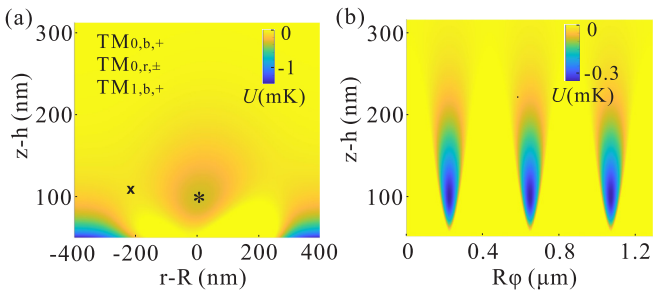

FIG. 3. The optical trap formed with hybrid modes. (a) The optical trap potential well above the microring surface in the r-z plane. (b) The optical trap potential well in the z-ϕ plane with $r - R = 6$ nm above the microring surface.

4.3 mW, and the blue-detuned TM_1 mode power is $P_{b1} = 1.8$ mW. With red-detuned TM_0 modes bidirectionally excited and other waveguide modes unidirectionally excited, a standing wave of the red-detuned TM_0 modes is formed in the ϕ direction. An array of optical trap wells with a trap depth of approximately 0.34 mW is formed in the z-ϕ plane on top of the microring waveguide, as shown in Fig. 3(b). The trap center in the ϕ direction is related to the phase difference of the two bidirectional excited red-detuned TM_0 modes. Thus, a stable atom trapping in three dimensions can be realized by hybrid mode trapping on the platform based on a suspension-free GaN-on-sapphire chip.

Furthermore, the relations between $U_{\rm eff}$ and P_r/P_b for different P_b are provided in Fig. 4(a). The trap depth increases at first and then decreases sharply with P_r/P_b to form a maximum optical trap depth with an optimal P_r/P_b for a given P_b. Both the optical trap depth and the optimal P_r/P_b increase with P_b. The asymmetry field distribution of TM_{0b} is made up of the TM_{1b} mode in the scheme of the hybrid modes. The trap potential on the saddle increases, which results in a large trap depth. The total mode power in the hybrid-mode-trapping scheme is reduced by one order of magnitude compared with the trapping scheme using the fundamental modes. Like in Fig. 2(c), a large P_r/P_b to overcome the van der Waals force forms a maximum trap potential for a fixed P_{b1}; thus, the optimal P_r/P_b increases with P_b. The total mode power in the hybrid-mode-trapping scheme is reduced by one order of magnitude compared with the trapping scheme using the fundamental modes. With reduced incident light power, the potential thermal effect or mechanical vibration of the microring will be greatly suppressed, which makes the optical trapping more stable. Then a stable atom trap can be realized on the plane perpendicular to the microring waveguide.

The relation between the optical trap depth $U_{\rm eff}$ and P_r/P_b with $P_b = 15$ mW is given in Fig. 4(b), where different curves correspond to different P_{b1}. With increased P_r/P_b, the optical trap depth $U_{\rm eff}$ increases at first and then decreases after a maximum $U_{\rm eff}$. From the different curves, the optical trap depth $U_{\rm eff}$ is larger with a larger P_{b1}, as is the maximum $U_{\rm eff}$. A larger P_{b1} can provide a stronger repulsive force, which results in a higher optimal P_r for a given P_b to achieve a balance between attractive and repulsive forces. The inset in Fig. 4(b) gives the relation between the optical trap depth and the blue-detuned TM_1 mode power P_{b1} with $P_b = 15$ mW

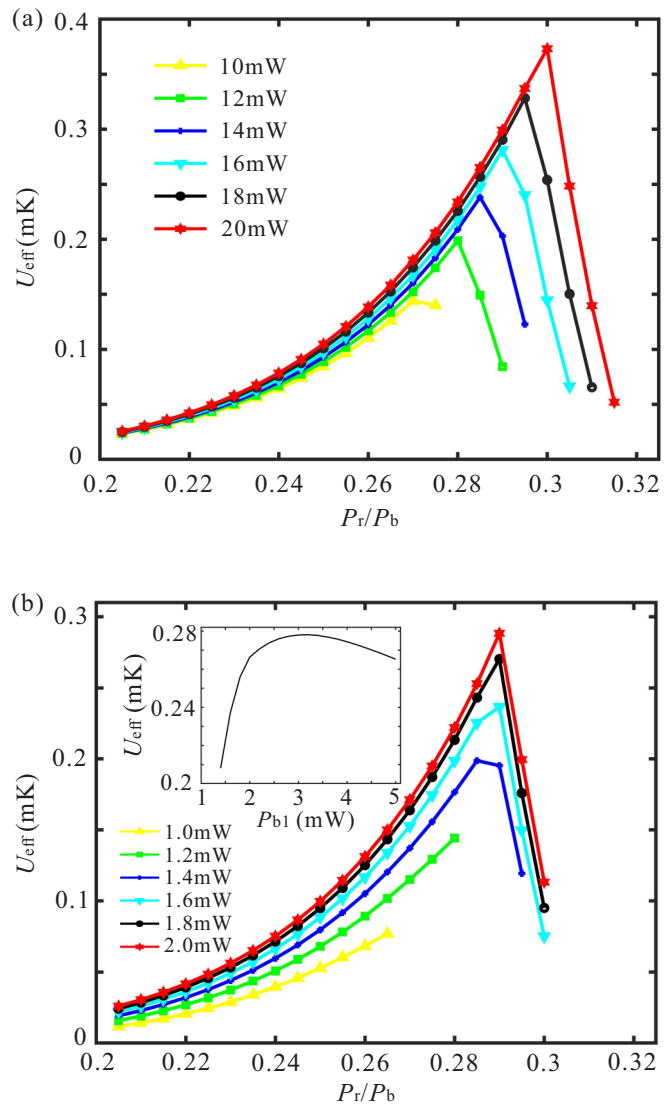

FIG. 4. (a) The optical traps vary with P_r/P_b for different P_b, with $P_{b1} = 1.8$ mW. (b) The optical traps vary with P_r/P_b for different P_{b1}, with $P_b = 15$ mW. The inset gives the relation between the optical trap and P_{b1}, with $P_b = 15$ mW and $P_r/P_b = 0.287$.

and $P_r/P_b = 0.287$. As the power of the blue-detuned TM_1 mode P_{b1} increases, the optical trap depth increases quickly at first to reach a maximum and then decreases slowly. Thus, an appropriate P_b makes the optical trap depth more efficient and regular and thus stable and requires low power consumption.

For the excitation of microring modes, three straight waveguides can be designed along the microring to couple red-detuned TM_0 and blue-detuned TM_0 and TM_1. The selective coupling between the propagating mode in the straight waveguide and the microring mode can be controlled by the width of the waveguide [51,52]. Therefore, the red-detuned TM_0 and blue-detuned TM_0 and TM_1 modes can be excited selectively.

IV. PHOTON-ATOM INTERACTION

The evanescent field around the microring waveguide interacts with the atoms trapped around the microring waveguide.

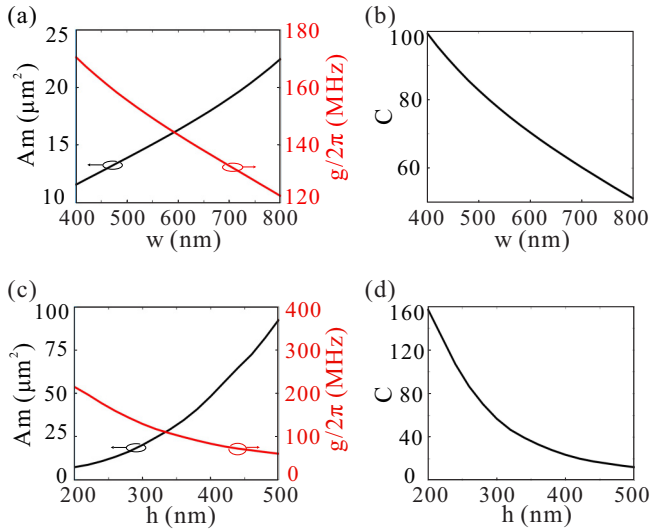

FIG. 5. The performance of the microcavity-enhanced atom-photon interaction of ^{87}Rb in the trap center $T(r = R, z - h = 100\,\text{nm})$. (a) The mode area A_m and coupling strength g and (b) cooperativity C vary with the waveguide width w of the microring with radius $R = 10\,\mu\text{m}$ and $h = 280\,\text{nm}$. (c) The mode area A_m and coupling strength g and (d) cooperativity C vary with the waveguide height w of the microring with $R = 10\,\mu\text{m}$ and $w = 600\,\text{nm}$.

Benefiting from the low loss of GaN and excellent processing technology, the photonic loss rate κ can be smaller than the photon-atom coupling strength g, as can the atomic radiative decay rate γ in free space. Thus, the photon-atom strong-coupling regime is potentially achievable with the current platform. For a perfect quantum emitter, the photon-atom coupling strength can be given as [27,53]

$$g = \sqrt{\frac{3\lambda^3\omega_0\gamma}{16\pi^2 V_m}}, \tag{1}$$

where λ is the free-space wavelength and ω_0 is the frequency of the photon mode. $\gamma/2\pi \approx 6.1\,\text{MHz}$ is the spontaneous emission rate of the atom in vacuum, i.e., equal to the angular frequency of the natural linewidth. V_m denotes the effective mode volume and can be derived to be approximately $V_m \approx 2\pi R A_m$ for a microring structure with a radius of R, and A_m is the effective mode area. For an atom located at working point (r_0, z_0),

$$A_m(r, z) = \frac{\int \varepsilon(r, z)|E(r, z)|^2 dr dz}{\varepsilon(r_0, z_0)|E(r_0, z_0)|^2}, \tag{2}$$

where $E(r, z)$ is the electric-field distribution and ε is the distribution of the dielectric permittivity.

Therefore, the merit of the quantum coherence of the microcavity-enhanced atom-photon interaction can be determined by the cooperativity parameter as

$$C = \frac{g^2}{\kappa\gamma} = \frac{3\lambda^3}{4\pi^2}\frac{Q}{V_m}, \tag{3}$$

where λ is the wavelength of light in free space. The cooperativity parameter mainly depends on the ratio of the quality factor Q and effective mode volume V_m. High cooperativity is pursued for a high-fidelity quantum gate between atoms and photons and potential nonlinear optical effects at single-photon levels. Additionally, the enhanced photon-atom interaction can also be applied to single-photon sources, with the cavity-enhanced collection efficiency of the radiation from the atomic quantum emitter

$$\eta = \frac{C}{1 + C}. \tag{4}$$

Note that C is equivalent to the Purcell factor, and the estimation of η is valid only in the bad-cavity limit with $g < \kappa$ [54]. If g is too strong, we can increase the cavity linewidth by introducing a higher external coupling rate to the microring cavity to meet the bad-cavity limit.

As noted in the last section, the two-color optical dipole trap can be constructed, and it is feasible to trap single atoms on top of the waveguide around $T(r = R, z - h = 100\,\text{nm})$. We are targeting the strong atom-photon interaction; thus, we focus on the fundamental mode polarized along the z direction at the wavelength of the D_2 transitions of the rubidium atom ($\sim$780 nm). For a GaN microring with a radius of a few tens of micrometers, the quality factor Q is mainly decided by the material absorption and scattering loss, and $Q = 2 \times 10^6$ with the corresponding $\kappa/2\pi \approx 100\,\text{MHz}$ taken in the simulations [35,47].

Figure 5 summarizes the performance of the microcavity-enhanced atom-photon interaction in the trap center $T(r = R, z - h = 100\,\text{nm})$ above the microring with different geometric parameters w and h. Although the waveguide geometry will affect the position of the trap center (see Appendix B), it is still possible to position the trap center around $T(r = R, z - h = 100\,\text{nm})$ using an appropriate power of the red- and blue-detuned modes. The effective mode area A_m and the photon-atom coupling strength g for ^{87}Rb and the microring with $R = 10\,\mu\text{m}$ and $h = 280\,\text{nm}$ are given in Fig. 5(a). The effective mode area A_m increases with increasing waveguide width since a wide waveguide constrains more mode field inside the waveguide with less mode field outside. With an increasing effective mode area A_m, the photon-atom coupling strength g decreases. The cooperativity parameter C of the ^{87}Rb atom also decreases with increasing waveguide width w of the microring, as shown in Fig. 5(b). The photon-atom interaction is also related to the waveguide height, as shown in Figs. 5(c) and 5(d) for the microring with $R = 10\,\mu\text{m}$ and $w = 600\,\text{nm}$. The effective mode area A_m increases, and the photon-atom coupling strength g decreases as the waveguide height h increases since a thicker waveguide has less evanescent field outside. The cooperativity parameter C of the ^{87}Rb atom also decreases as the waveguide height h increases.

From the above analysis, the photon-atom interaction increases as the size of the microring waveguide decreases. At the same time, the mode loss of the microring cavity increases as the size of the waveguide decreases. Therefore, an appropriate size of the microring waveguide is important to guarantee efficient photon-atom interactions. Table I gives the photon-atom interaction in the optical trap center $T(r - R, z - h = 100\,\text{nm})$ above the GaN microring waveguide for different parameters. The power of the blue-detuned modes is $P_b = 15\,\text{mW}$ and $P_{b1} = 1.8\,\text{mW}$. It is shown that the depth of the optical trap well is larger than 0.1 mk, which can trap a

TABLE I. The photon-atom interaction of ^{87}Rb in the trap well formed above the GaN microring waveguide with intracavity trap laser power $P_b = 15$ mW, $P_{b1} = 1.8$ mW, and microring radius $R = 10\,\mu$m.

w (μm)	0.7	0.6	0.6	0.6	0.6
h (μm)	0.28	0.32	0.3	0.28	0.26
P_r/P_b	0.277	0.264	0.268	0.287	0.3011
$T(r-R, z-h)$ (nm, nm)	(4, 100)	(−5, 100)	(−26, 100)	(6,100)	(7,100)
U_{min} (mK)	−0.287	−0.213	−0.253	−0.344	−0.431
U_{eff} (mK)	0.180	0.107	0.112	0.256	0.331
A_m (μm^2)	18.89	24.84	21.47	16.14	13.10
$g/2\pi$ (MHz)	133.5	116.4	125.2	144.4	160.3
C	60.83	46.26	53.51	71.19	87.68

single atom stably. At the same time, the trapped atom has an efficient photon-atom interaction with microring waveguide modes. The photon-atom coupling strength $g/2\pi$ is larger than 110 MHz, and the cooperativity parameter C is larger than 42, with the corresponding collection efficiency being above 97.7%. Since the $TM_{b,1}$ mode is used to improve the trap of the atom, the cutoff of the TM_1 mode is provided in Fig. 6. For a small waveguide width w and height h, the TM_1 mode can be excited and propagate well in the microring waveguide. Therefore, the proposed platform based on a suspension-free GaN-on-sapphire chip is feasible for providing stable atom trapping with hybrid modes for the photon-atom interaction in the integrated quantum information.

V. CONCLUSION

A stable platform for trapping atoms was proposed to realize the hybrid photon-atom circuit based on a suspension-free GaN-on-sapphire chip. The high-order waveguide modes were used to realize a stable trap potential well with low incident trap light power, with which a feasible and regular dipole trap potential well around 300 μK can be obtained with only 10-mW-level power circulating in the microring (equivalently, sub-milliwatt-level input power in the coupling waveguide). In addition, the interaction between trapped atoms and guided photons in the resonator was analyzed to confirm a high-cooperativity photon-atom interface for potential applications. Such a stable on-chip atom trapping scheme will play a key role in the hybrid photon-atom circuit, which provides a unique experimental platform for studying quantum optics effects with novel photonic structures, single-photon-level nonlinear photonics, and quantum devices for scalable quantum information processing [9].

ACKNOWLEDGMENTS

This work was supported by the National Key Research and Development Program of China (Grants No. 2018YFA0306400 and No. 2017YFA0304100), the National Natural Science Foundation of China (Grants No. 11922411, No.U21A6006, No. 12104441, No. 12134014, No. 12074194, and No. 12124014), a project funded by the China Postdoctoral Science Foundation (2019M651911), the Leading-edge Technology Program of Jiangsu Natural Science Foundation (Grant No. BK20192001 and No. BE2022071), the USTC Research Funds of the Double First-Class Initiative (Grant No. YD2030002007), and the Fund for Shanxi "1331 Project" Key Subjects Construction. C.-L.Z. was also supported by the Fundamental Research Funds for the Central Universities and the Program of State Key Laboratory of Quantum Optics and Quantum Optics Devices. This work was partially carried out at the USTC Center for Micro and Nanoscale Research and Fabrication.

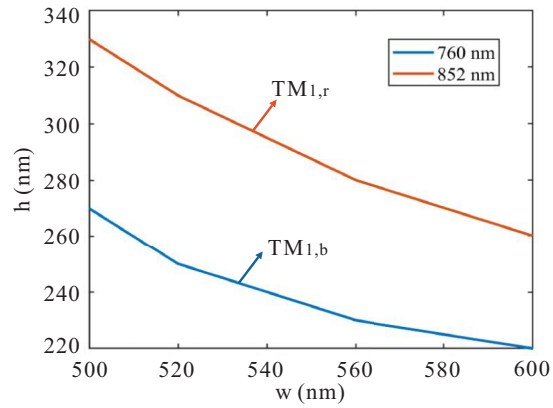

FIG. 6. The cutoff condition of the TM_1 mode for the blue- and red-detuned wavelengths. The lines indicate the critical parameters for the cutoff condition, and the mode is allowed only when the h and w parameters are above the critical line.

APPENDIX A: CALCULATION OF THE TRAPPING POTENTIAL

In an electric field E with a far-off-resonant trap, a neutral atom experiences an ac stark shift. The potential depth can be given as [53,55]

$$U_{od} = \frac{I(r,z)\pi c^2}{2\omega_0^3}\left[\left(\frac{\gamma_1}{\omega_0-\omega_1} + 2\frac{\gamma_2}{\omega_0-\omega_2}\right) - g_F\left(\frac{\gamma_1}{\omega_0-\omega_1} - 2\frac{\gamma_2}{\omega_0-\omega_2}\right)\mathbf{e}(r,z)\cdot\mathbf{F}\right], \quad \text{(A1)}$$

where the natural linewidths $\gamma_1 = 2\pi \times 5.75$ MHz and $\gamma_2 = 2\pi \times 6.07$ MHz for lines D_1 and D_2 in ^{87}Rb and $\mathbf{e}(r,z)$ is the ellipticity. $I(r,z)$ is the evanescent intensity. $g_F = [F(F+1) + S(S+1) - I(I+1)]/[F(F+1)]$ is the Landé g factor. $\mathbf{F}$ is the total angular momentum operator. Taking $m_F = 0$ for

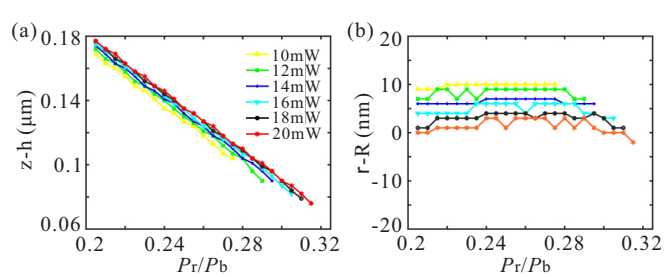

FIG. 7. The trap center as a function of P_r/P_b for different P_b values corresponding to Fig. 3(a). (a) z direction and (b) r direction.

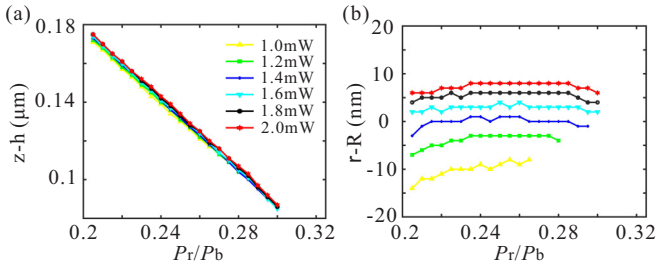

FIG. 8. The trap center as a function of P_r/P_b for different P_{b1} values corresponding to Fig. 3(b). (a) z direction and (b) r direction

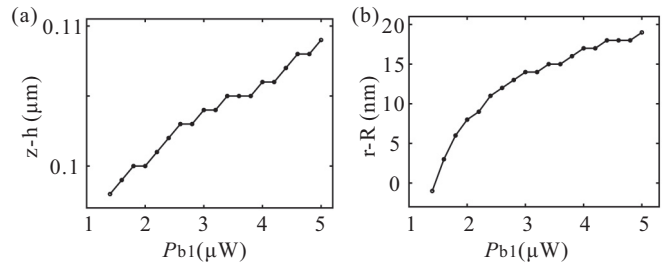

FIG. 9. The trap center as a function of P_{b1} corresponding to the inset in Fig. 3(b). (a) z direction and (b) r direction.

simplicity, the potential depth (A1) can be given as

$$U_{\rm od} = \frac{I(r,z)\pi c^2}{2\omega_0^3}\left[\left(\frac{\gamma_1}{\omega_0-\omega_1}+2\frac{\gamma_2}{\omega_0-\omega_2}\right)\right]. \tag{A2}$$

When the atom approximates to the waveguide surface with submicron distances, there is a van der Waals potential [48]

$$U_{\rm vdW} = 0.12\frac{\hbar\gamma\lambda^3}{(2\pi)^3(z-h_1)^3}. \tag{A3}$$

In the calculation of the optical trap potential, a ground-state ^{87}Rb atom placed above a microring waveguide is considered to have a two-color strong evanescent field. The 760- and 852-nm blue- and red-detuned lights are far off resonant from the atomic resonances. The total potential is the sum of the optical dipole potential and the van der Waals potential, which can be given as

$$U = U_{\rm or} + U_{\rm ob} + U_{\rm vdW}. \tag{A4}$$

APPENDIX B: THE SHIFT OF THE TRAP CENTER

When P_r/P_b and P_{b1} are changed, the trap center will be shifted. The trap center as a function of P_r/P_b and P_{b1} is shown in Figs. 7–9.

[1] J.-H. Kim, S. Aghaeimeibodi, J. Carolan, D. Englund, and E. Waks, Hybrid integration methods for on-chip quantum photonics, Optica **7**, 291 (2020).

[2] A. W. Elshaari, W. Pernice, K. Srinivasan, O. Benson, and V. Zwiller, Hybrid integrated quantum photonic circuits, Nat. Photonics **14**, 285 (2020).

[3] E. Pelucchi, G. Fagas, I. Aharonovich, D. Englund, E. Figueroa, Q. Gong, H. Hannes, J. Liu, C.-Y. Lu, N. Matsuda, J.-W. Pan, F. Schreck, F. Sciarrino, C. Silberhorn, J. Wang and K. D. Jöns, The potential and global outlook of integrated photonics for quantum technologies, Nat. Rev. Phys. **4**, 194 (2021).

[4] D. Dai, J. Bauters, and J. E. Bowers, Passive technologies for future large-scale photonic integrated circuits on silicon: Polarization handling, light non-reciprocity and loss reduction, Light: Sci. Appl. **1**, e1 (2012).

[5] W. Bogaerts, D. Pérez, J. Capmany, D. A. B. Miller, J. Poon, D. Englund, F. Morichetti, and A. Melloni, Programmable photonic circuits, Nature (London) **586**, 207 (2020).

[6] B. J. Shastri, A. N. Tait, T. Ferreira de Lima, W. H. P. Pernice, H. Bhaskaran, C. D. Wright, and P. R. Prucnal, Photonics for artificial intelligence and neuromorphic computing, Nat. Photonics **15**, 102 (2021).

[7] S. Y. Siew, B. Li, F. Gao, H. Y. Zheng, W. Zhang, P. Guo, S. W. Xie, A. Song, B. Dong, L. W. Luo, C. Li, X. Luo, and G.-Q. Lo, Review of silicon photonics technology and platform development, J. Lightwave Technol. **39**, 4374 (2021).

[8] H. J. Kimble, The quantum internet, Nature (London) **453**, 1023 (2008).

[9] D. E. Chang, J. S. Douglas, A. González-Tudela, C.-L. Hung, and H. J. Kimble, Colloquium: Quantum matter built from nanoscopic lattices of atoms and photons, Rev. Mod. Phys. **90**, 031002 (2018).

[10] C. L. Garrido Alzar, Compact chip-scale guided cold atom gyrometers for inertial navigation: Enabling technologies and design study, AVS Quantum Sci. **1**, 014702 (2019).

[11] B. Dayan, A. Parkins, T. Aoki, and E. Ostby, A photon turnstile dynamically regulated by one atom, Science **319**, 1062 (2008).

[12] I. Shomroni, S. Rosenblum, Y. Lovsky, O. Bechler, G. Guendelman, and B. Dayan, All-optical routing of single photons by a one-atom switch controlled by a single photon, Science **345**, 903 (2014).

[13] J. Volz, M. Scheucher, C. Junge, and A. Rauschenbeutel, Nonlinear π phase shift for single fibre-guided photons interacting with a single resonator-enhanced atom, Nat. Photonics **8**, 965 (2014).

[14] N. V. Corzo, J. Raskop, A. Chandra, A. S. Sheremet, B. Gouraud, and J. Laurat, Waveguide-coupled single collective excitation of atomic arrays, Nature (London) **566**, 359 (2019).

[15] M. Daly, V. G. Truong, C. Phelan, K. Deasy, and S. N. Chormaic, Nanostructured optical nanofibres for atom trapping, New J. Phys. **16**, 053052 (2014).

[16] Y. Meng, C. Liedl, S. Pucher, A. Rauschenbeutel, and P. Schneeweiss, Imaging and Localizing Individual Atoms Interfaced with a Nanophotonic Waveguide, Phys. Rev. Lett. **125**, 053603 (2020).

[17] A. Goban, C.-L. Hung, S.-P. Yu, J. D. Hood, J. a. Muniz, J. H. Lee, M. J. Martin, A. C. McClung, K. S. Choi, D. E. Chang, O. Painter, and H. J. Kimble, Atom-light interactions in photonic crystals. Nat. Commun. **5**, 3808 (2014).

[18] X. Luan, J.-B. Béguin, A. P. Burgers, Z. Qin, S.-P. Yu, and H. J. Kimble, The integration of photonic crystal waveguides with atom arrays in optical tweezers, Adv. Quantum Technol. **3**, 2000008 (2020).

[19] J.-B. Béguin, Z. Qin, X. Luan, and H. Kimble, Coupling of light and mechanics in a photonic crystal waveguide, Proc. Natl. Acad. Sci. USA **117**, 29422 (2020).

[20] M. Gehl, W. Kindel, N. Karl, A. Orozco, K. Musick, D. Trotter, C. Dallo, A. Starbuck, A. Leenheer, C. DeRose, G. Biedermann, Y.-Y. Jau, and J. Lee, Characterization of suspended membrane waveguides towards a photonic atom trap integrated platform, Opt. Express **29**, 13129 (2021).

[21] T. Tiecke, J. D. Thompson, N. P. de Leon, L. Liu, V. Vuletić, and M. D. Lukin, Nanophotonic quantum phase switch with a single atom, Nature (London) **508**, 241 (2014).

[22] P. Samutpraphoot, T. Đorđević, P. L. Ocola, H. Bernien, C. Senko, V. Vuletić, and M. D. Lukin, Strong Coupling of Two Individually Controlled Atoms via a Nanophotonic Cavity, Phys. Rev. Lett. **124**, 063602 (2020).

[23] T. Đorđević, P. Samutpraphoot, P. L. Ocola, H. Bernien, B. Grinkemeyer, I. Dimitrova, V. Vuletić, and M. D. Lukin, Entanglement transport and a nanophotonic interface for atoms in optical tweezers, Science **373**, 1511 (2021).

[24] E. Will, L. Masters, A. Rauschenbeutel, M. Scheucher, and J. Volz, Coupling a Single Trapped Atom to a Whispering-Gallery-Mode Microresonator, Phys. Rev. Lett. **126**, 233602 (2021).

[25] M. Kohnen, M. Succo, P. G. Petrov, R. A. Nyman, M. Trupke, and E. A. Hinds, An array of integrated atom–photon junctions, Nat. Photonics **5**, 35 (2011).

[26] Y. Meng, J. Lee, M. Dagenais, and S. L. Rolston, A nanowaveguide platform for collective atom-light interaction, Appl. Phys. Lett. **107**, 091110 (2015).

[27] T.-H. Chang, B. M. Fields, M. E. Kim, and C.-L. Hung, Microring resonators on a suspended membrane circuit for atom–light interactions, Optica **6**, 1203 (2019).

[28] M. E. Kim, T.-H. Chang, B. M. Fields, C.-A. Chen, and C.-L. Hung, Trapping single atoms on a nanophotonic circuit with configurable tweezer lattices, Nat. Commun. **10**, 1647 (2019).

[29] T.-H. Chang, X. Zhou, M. Zhu, B. M. Fields, and C.-L. Hung, Efficiently coupled microring circuit for on-chip cavity QED with trapped atoms, Appl. Phys. Lett. **117**, 174001 (2020).

[30] X. Zhou, H. Tamura, T.-H. Chang, and C.-L. Hung, Subwavelength precision optical guiding for trapped atoms coupled to a nanophotonic resonator, arXiv:2111.01119

[31] Y. Zhang, L. McKnight, E. Engin, I. M. Watson, M. J. Cryan, E. Gu, M. G. Thompson, S. Calvez, J. L. O'Brien, and M. D. Dawson, GaN directional couplers for integrated quantum photonics, Appl. Phys. Lett. **99**, 161119 (2011).

[32] A. W. Bruch, C. Xiong, B. Leung, M. Poot, J. Han, and H. X. Tang, Broadband nanophotonic waveguides and resonators based on epitaxial GaN thin films, Appl. Phys. Lett. **107**, 141113 (2015).

[33] H. Chen, H. Fu, X. Huang, X. Zhang, T.-H. Yang, J. A. Montes, I. Baranowski, and Y. Zhao, Low loss GaN waveguides at the visible spectral wavelengths for integrated photonics applications, Opt. Express **25**, 31758 (2017).

[34] K. H. Li, Y. F. Cheung, W. Y. Fu, K. K.-Y. Wong, and H. W. Choi, Monolithic Integration of GaN-on-sapphire light-emitting diodes, photodetectors, and waveguides, IEEE J. Sel. Top. Quantum Electron. **24**, 3801706 (2018).

[35] E. Stassen, M. Pu, E. Semenova, E. Zavarin, W. Lundin, and K. Yvind, High-confinement gallium nitride-on-sapphire waveguides for integrated nonlinear photonics, Opt. Lett. **44**, 1064 (2019).

[36] W. Fu, Z. Shen, Y. Xu, C.-L. Zou, R. Cheng, X. Han, and H. X. Tang, Phononic integrated circuitry and spin-orbit interaction of phonons, Nat. Commun. **10**, 2743 (2019).

[37] X.-B. Xu, J.-Q. Wang, Y.-H. Yang, W. Wang, Y.-L. Zhang, B.-Z. Wang, C.-H. Dong, L. Sun, G.-C. Guo, and C.-L. Zou, High-frequency traveling-wave phononic cavity with sub-micron wavelength, Appl. Phys. Lett. **120**, 163503 (2022).

[38] D. Schrader, S. Kuhr, W. Alt, M. Müller, V. Gomer, and D. Meschede, An optical conveyor belt for single neutral atoms, Appl. Phys. B **73**, 819 (2001).

[39] S. Kuhr, W. Alt, D. Schrader, M. Muller, V. Gomer, and D. Meschede, Deterministic delivery of a single atom, Science **293**, 278 (2001).

[40] F. Le Kien, V. I. Balykin, and K. Hakuta, Atom trap and waveguide using a two-color evanescent light field around a subwavelength-diameter optical fiber, Phys. Rev. A **70**, 063403 (2004).

[41] E. Vetsch, D. Reitz, G. Sagué, R. Schmidt, S. T. Dawkins, and A. Rauschenbeutel, Optical Interface Created by Laser-Cooled Atoms Trapped in the Evanescent Field Surrounding an Optical Nanofiber, Phys. Rev. Lett. **104**, 203603 (2010).

[42] J. Fu, X. Yin, and L. Tong, Two-colour atom guide and 1d optical lattice using evanescent fields of high-order transverse modes, J. Phys. B **40**, 4195 (2007).

[43] K. Padmaraju, J. Chan, L. Chen, M. Lipson, and K. Bergman, Thermal stabilization of a microring modulator using feedback control, Opt. Express **20**, 27999 (2012).

[44] K. Padmaraju and K. Bergman, Resolving the thermal challenges for silicon microring resonator devices, Nanophotonics **3**, 269 (2014).

[45] G. Yu, G. Wang, H. Ishikawa, M. Umeno, T. Soga, T. Egawa, J. Watanabe, and T. Jimbo, Optical properties of wurtzite structure GaN on sapphire around fundamental absorption edge (0.78–4.77 eV) by spectroscopic ellipsometry and the optical transmission method, Appl. Phys. Lett. **70**, 3209 (1997).

[46] J. F. Muth, J. D. Brown, M. A. L. Johnson, Z. Yu, R. M. Kolbas, J. W. Cook, Jr., and J. F. Schetzina, Absorption coefficient and refractive index of GaN, AlN and AlGaN alloys, MRS Internet J. Nitride Semicond. Res. **4**, 502 (1999).

[47] Y. Zheng, C. Sun, B. Xiong, L. Wang, Z. Hao, J. Wang, Y. Han, H. Li, J. Yu, and Y. Luo, Integrated gallium nitride nonlinear photonics, Laser Photonics Rev. **16**, 2100071 (2022).

[48] A. McLachlan, Van der Waals forces between an atom and a surface, Mol. Phys. **7**, 381 (1964).

[49] X. Ji, J. K. Jang, U. D. Dave, M. Corato-Zanarella, C. Joshi, A. L. Gaeta, and M. Lipson, Exploiting ultralow loss multimode waveguides for broadband frequency combs, Laser Photonics Rev. **15**, 2000353 (2021).

[50] C. Phelan, T. Hennessy, and T. Busch, Shaping the evanescent field of optical nanofibers for cold atom trapping, Opt. Express **21**, 27093 (2013).

[51] L.-W. Luo, N. Ophir, C. P. Chen, L. H. Gabrielli, C. B. Poitras, K. Bergmen, and M. Lipson, WDM-compatible mode-division multiplexing on a silicon chip, Nat. Commun. **5**, 3069 (2014).

[52] L.-T. Feng, M. Zhang, X. Xiong, Y. Chen, H. Wu, M. Li, G.-P. Guo, G.-C. Guo, D.-X. Dai, and X.-F. Ren, On-chip transverse-mode entangled photon pair source, npj Quantum Inf. **5**, 2 (2019).

[53] K. L. Corwin, S. J. M. Kuppens, D. Cho, and C. E. Wieman, Spin-Polarized Atoms in a Circularly Polarized Optical Dipole Trap, Phys. Rev. Lett. **83**, 1311 (1999).

[54] P. R. Berman, *Cavity Quantum Electrodynamics* (Academic, Boston, 1994).

[55] T. H. Stievater, D. A. Kozak, M. W. Pruessner, R. Mahon, D. Park, W. S. Rabinovich, and F. K. Fatemi, Modal characterization of nanophotonic waveguides for atom trapping, Opt. Mater. Express **6**, 3826 (2016).